

# Nanoscale

Accepted Manuscript



This is an *Accepted Manuscript*, which has been through the Royal Society of Chemistry peer review process and has been accepted for publication.

*Accepted Manuscripts* are published online shortly after acceptance, before technical editing, formatting and proof reading. Using this free service, authors can make their results available to the community, in citable form, before we publish the edited article. We will replace this *Accepted Manuscript* with the edited and formatted *Advance Article* as soon as it is available.

You can find more information about *Accepted Manuscripts* in the [Information for Authors](#).

Please note that technical editing may introduce minor changes to the text and/or graphics, which may alter content. The journal's standard [Terms & Conditions](#) and the [Ethical guidelines](#) still apply. In no event shall the Royal Society of Chemistry be held responsible for any errors or omissions in this *Accepted Manuscript* or any consequences arising from the use of any information it contains.



## Nanoscale

## PAPER

## Facet-Controlled Facilitation of PbS Nanoarchitectures by Understanding Nanocrystal Growth

Welley Siu Loc,<sup>a,t</sup> Zewei Quan,<sup>a,t,▼</sup> Cuikun Lin,<sup>b</sup> Jinfong Pan,<sup>c</sup> Yuxuan Wang,<sup>c</sup> Kaikun Yang,<sup>d</sup> Wen-Bin Jian,<sup>e</sup> Bo Zhao,<sup>b</sup> Howard Wang<sup>d</sup> and Jiye Fang<sup>\*,a,c</sup>

Received 00th January 20xx,  
Accepted 00th January 20xx

DOI: 10.1039/x0xx00000x

www.rsc.org/

Nanostructured lead sulphide is a significant component in a number of energy-related sustainable applications such as photovoltaic cells and thermoelectric components. In many micro-packaging processes, dimensionality-controlled nanoarchitectures as building blocks with unique properties are required. This study investigates different facet-merging growth behaviors through a wet-chemical synthetic strategy to produce high-quality controlled nanostructures of lead sulphide in various dimensionalities. It is determined that the 1D nanowires or 2D nanosheets can be obtained by the merging of reactive {111}- or {110}-facets, respectively, while promoting {100} facets in early stages after nucleation leads to a growth of 0D nanocubes. The influence of temperature, capping ligands and co-solvent on facilitating crystal facet growth of each intermediate seed is demonstrated as well. The novelty of this work is characterized by the delicate manipulation of various PbS nanoarchitectures based on the comprehension of facet-merging evolutions. Synthesis of facet-controlled PbS nanostructures could provide novel building blocks with desired properties to be used in many applications.

### Introduction

Dimensionality-controlled fabrication of nanostructured semiconductors is not only significant for understanding shape-dependent properties, but also useful in a wide range of energy-related applications because electron confinement within a semiconductor nanocrystal (NC) provides the most powerful pathway to tune the electronic, optical and magnetic properties.<sup>1-3</sup> Among all available solid materials, lead chalcogenides deserve a prioritized consideration due to their unique characteristics such as relatively narrow band gaps and large Bohr exciton radii that enable strong quantum-confinement-effects.<sup>4,5</sup> Furthermore, lead chalcogenides hold promise for a large number of technological needs such as photovoltaic, thermoelectric and telecommunication

applications.<sup>6-9</sup> For example, it was reported that lead sulphide (PbS) photovoltaic cells could generate a higher open-circuit voltage compared to lead selenide (PbSe) which possesses larger short circuit photocurrents when the band gap is similar.<sup>10,11</sup> PbS nanocubes have recently been packed into thin films on a flexible substrate for photovoltaic application.<sup>12</sup> These fascinating features have prompted intensive study on the design and synthesis of lead chalcogenide NCs with well-defined architectures, and many strategies for controlling the size, shape and attachment of NCs have been developed.<sup>12-22</sup> However, most synthetic studies were focused on a specific dimension and there is a lack in developing a unified set of synthesis method as well as deep comprehension on the crystal growth to achieve versatile dimensionalities of these nanostructured lead chalcogenides.

In this work, we report a recently developed shape-controlled synthesis strategy, in which the growth of PbS nanostructures can be branched out to three distinctive paths, resulting in a formation of one-dimensional nanowires (1D NWs), two-dimensional nanosheets (2D NSs), and zero-dimensional nanoparticles (0D NPs) including nanocubes (NCBs) and nanocubo-octahedra (NCOs), respectively. In order to understand the formation nature of various PbS nanostructures, the effect of specific reaction parameters such as the type of capping ligands, growth temperature and reaction time on the final morphology was systematically investigated. A mechanism associated with the facet-dependent nanostructure growth was subsequently proposed. This work provides a general method and understanding of shape-controlled PbS nanoarchitectures that could serve various emerging energy-related nanodevices.

<sup>a</sup> Department of Chemistry, State University of New York at Binghamton, Binghamton, New York 13902, United States; E-mail: jfang@binghamton.edu.

<sup>b</sup> Department of Chemistry, University of South Dakota, Vermillion, South Dakota, United States.

<sup>c</sup> Materials Science and Engineering Program, State University of New York at Binghamton, Binghamton, New York 13902, United States.

<sup>d</sup> Department of Mechanical Engineering, State University of New York at Binghamton, Binghamton, New York 13902, United States.

<sup>e</sup> Department of Electrophysics, National Chiao Tung University, Hsinchu 30010, Taiwan, ROC

† W.S.L. and Z.Q. contributed equally.

▼ Present Address: Earth and Environmental Science Division, Los Alamos National Laboratory, Los Alamos, New Mexico 87545, United States

Electronic Supplementary Information (ESI) available: Experimental section (chemicals, synthesis, characterization methods), synthesis conditions, AFM image of NSs, SEM and TEM images of NWs prepared without OAm, and TEM images of truncated NCBs grown for 7.5 min at 180 °C. See DOI: 10.1039/x0xx00000x

## Results and Discussion

PbS nanostructures were prepared in a standard air-free Schlenk line system under an argon stream. The detailed recipe for each synthesis is documented in Supporting Information (SI). In brief, to prepare PbS 1D NWs, Pb-oleate that was pre-prepared by dissolving PbO into a mixture of hot diphenyl ether (DPE) and oleic acid (OA), was transferred into a three-neck round-bottom flask containing oleylamine (OAm) and DPE at ambient conditions. After the mixture was heated to 180 °C, certain amount of sulphur-triethylphosphine (S-TOP) was injected into the flask. After 5.0 min, the heating source was removed and the flask was immediately immersed into a cold water bath.<sup>19, 23</sup> The resultant PbS NWs were washed and isolated using a standard procedure as described in SI. Synthesis of PbS 2D NSs was similarly carried out at 150 °C. After the addition of S-TOP (10 sec), 1,2-dichloroethane (DCE) was subsequently injected into the system, and the growth was allowed to proceed for 7.5 min. PbS 0D NCBs were prepared at 200 °C using a similar recipe to 1D NWs, but sulphur-oleylamine (S-OAm) was used in place of the S-TOP precursor. To prepare PbS 0D NCOs, all procedures are identical except for an immediate addition of DCE following the injection of S-OAm solution. For ease of comparison, synthetic parameters of PbS 0D NPs, 1D NWs and 2D NSs are presented in Table S1 in SI.

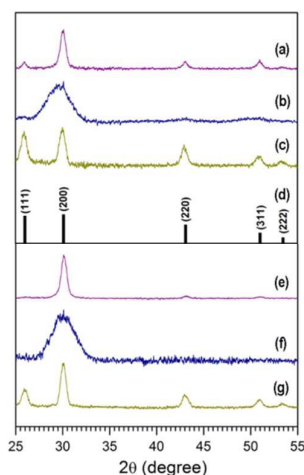


**Figure 1.** XRD patterns of PbS nanostructures. (a,e) 1D NWs, (b,f) 2D NSs, (c,g) 0D NPs; (a-c) samples were randomly deposited on a PANalytical zero-background Si sample holder, (e-g) samples were assembled on a surface-polished Si wafer; (d) standard pattern from ICDD PDF card (78-1901).

Figure 1 presents XRD patterns of the as-prepared 1D NWs, 2D NSs and 0D NPs of PbS products on a PANalytical zero-background Si sample holder (Figure 1a-1c) and on a surface-polished Si wafer (Figure 1e-1g), respectively. The detectable peaks from patterns of these three samples can be assigned to those of a face-centred cubic (fcc) PbS crystal (ICDD PDF card No. 78-1901,  $Fm\bar{3}m$ , Figure 1d). Diffraction peaks (111) at  $2\theta = 25.998^\circ$  and (200) at  $2\theta = 30.108^\circ$  are used to primarily compare the preferred orientation in each nanostructure, by comparing the ratio (denoted as  $i$ ) of their relative intensities with that in the standard pattern. Within the XRD pattern of

the NWs (Figure 1a), the intensity of (111) peak is significantly weaker than the (200), giving  $i = 0.18$  or  $0.11$ , respectively, vs  $i = 0.95$  in the standard ICDD card. This indicates that the 1D NWs have a preferential orientation along the (100) axis.<sup>14</sup> The (220) diffraction peak is absent in pattern of 2D NSs (Figure 1b), which suggests that the growth direction could be parallel to the  $\langle 110 \rangle$  axes. When both samples were self-assembled onto a surface-polished Si substrate, the (111), (220), (311) and (222) diffraction peaks are relatively absent because of unique texture effects corresponding to NWs/NSs that are aligned parallel to the substrate<sup>18, 24</sup> (Figure 1e and 1f). This is not the case in the 0D NPs that are slightly truncated NCBs (*vide infra*), as shown in Figure 1c and 1g. The value of  $i$  in Figure 1c is 0.85, compared to a value of 0.95 in the standard card. Since the building blocks are not perfect NCBs, the building blocks are not orderly packed onto the surface-polished Si wafer substrate, and the value of  $i$  is therefore not zero (Figure 1g).

Among the three nanoarchitectures, 2D NSs (Figure 1b and 1f) displayed the most apparent peak broadening effect, which is associated with their ultrathin feature. The crystallite sizes for the three classes of PbS nanostructures were estimated using the Scherer equation based on (200) diffraction peaks, giving the following average results:  $\sim 12$  nm in diameter for the 1D NWs;  $\sim 5$  nm in thickness for the 2D NSs; and  $\sim 14$  nm in side-length for the 0D slightly truncated NCBs. We have also alternatively measured the sizes using their TEM/AFM images, obtaining an average diameter of the NWs as  $11.3 \pm 2.1$  nm on the basis of 50 PbS NWS (TEM); an average thickness of the NSs as 5-7 nm (AFM, Figure S1); and an average side-length of the NCBs as  $15.8 \pm 1.7$  nm on the basis of  $\sim 200$  PbS NCBs (TEM). The actual thickness of the 2D NSs may be less than the reported value if the surfactant layer is considered.<sup>25</sup> The lengths of the NWs range from 200 nm to 1  $\mu\text{m}$  with a large distribution, and the widths of the NSs are within a broad range from 60 nm to 1  $\mu\text{m}$ . These results are in agreement with estimations obtained from the Scherer equation, implying that at least one dimensionality of the PbS NWs and NSs is confined within the length of PbS Bohr radius ( $\sim 20$  nm).<sup>5</sup>

The 1D NWs were immediately present after S-TOP was injected into the reaction mixture at temperatures of  $>150$  °C. TEM images of the PbS NWs grown at 180 °C at selected reaction stages are shown in Figure 2a-2d. The NWs in Figure 2a and 2b that were grown for 2 min and 4 min, respectively, have corrugated surface morphology with a zig-zag structure as observed before.<sup>26</sup> This is an indication that the formation of NWs began with PbS nanooctahedral crystals (or with slight truncation) enclosed by reactive {111} facets. As the growth time was increased to 5 min (Figure 2c) and 7.5 min (Figure 2d), the rough NW surface flattened out by competitive growth between the {100} and {111} facets of the fcc-structured PbS.<sup>27</sup> A further observation on the resultant zig-zag 1D nanostructures strongly suggests that the attachment of small nanooctahedra ( $\sim 5$  nm in diameter) can subsequently promote the formation of PbS NWs. It is known that the attachment of PbS nanooctahedra is irreversible at an elevated temperature, which is similar to a case of PbSe NCs reported

previously.<sup>14, 17</sup> The final shape of the 1D NWs can be determined by relative growth rates in  $\langle 100 \rangle$  and  $\langle 111 \rangle$  directions.<sup>28</sup> Upon an injection of the S-TOP precursor at temperatures of  $>150^\circ\text{C}$ , PbS NCs grow from NCO seeds with six  $\{100\}$  and eight  $\{111\}$  facets, as  $\{100\}$  facets vanish first due to their relatively faster growth rate along  $\langle 100 \rangle$  compared to that along  $\langle 111 \rangle$ . This results in a formation of the nanooctahedra with highly active  $\{111\}$  facets and their subsequent attachments as 1D zig-zag NWs, each of which is about two nanooctahedron-wide in diameter (Figure 2a and 2b) as expressed in the following steps:

$\{100\}$  facets  $\rightleftharpoons$   $\{111\}$  facets  $\rightarrow$  1D zig-zag NWs.

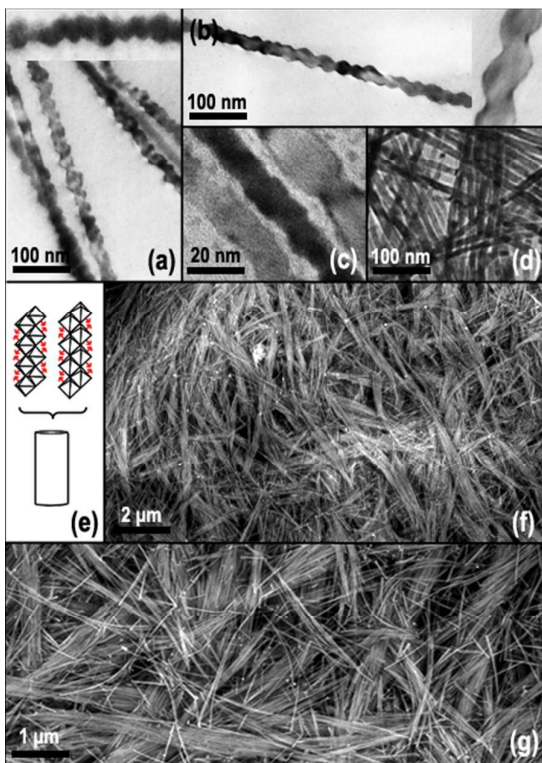


**Figure 2.** EM images of PbS 1D NWs grown at  $180^\circ\text{C}$ . (a-d) TEM images of 1D PbS NWs with growth time as 2 min, 4 min, 5 min, and 7.5 min, respectively; (e) schematic of two different NW conformations with different orientations in the nanooctahedron arrangement, and their transition process into a smooth NW; (f, g) SEM images of PbS NWs synthesized at  $180^\circ\text{C}$  for 5 min.

These 1D NWs contain nanooctahedra that are attached in two different ways by sharing  $\{111\}$  facets, that is, nanooctahedra stacked in a way of face-to-face horizontally and nanooctahedra assembled in a way of tip-to-tip vertically.<sup>29</sup> Referring to Figure 2e, it is speculated that the smoothing process of these zig-zag NWs grows out of the successive growth of  $\{111\}$  planes over time in order to lower their surface energy.<sup>30</sup> Highlighted in Figure 2f and 2g, the as-prepared PbS NWs displayed in Figure 2c can be self-assembled as arrays with a relatively uniform orientation on a Si substrate. In addition to the effect of the reaction kinetics, the feature of these PbS NWs is also associated with the amount of OAm used in the preparation. Under the reported conditions, the absence of OAm leads to a

heavy aggregation of the NWs as shown in Figure S2a in SI, implying that OAm penetrates to the surface to disperse the NWs. When one-tenth of the typical OAm volume (0.3 mL) was used, smooth 1D NWs and 2D NSs ( $\sim 150$  nm in width) could be co-produced (Figure S2b in SI).

Interestingly, obtaining mixed products suggests a connection between the 1D NW and 2D NS formation. At lower temperatures ( $\leq 150^\circ\text{C}$ ), 2D NS evolution was favoured. It was reported that a PbS NS could grow out of the merging of highly reactive  $\{110\}$  facets.<sup>24</sup> Our XRD determinations also supports this finding. Given that  $\{110\}$  facets on small sized PbSe NCs are high surface energy planes<sup>14</sup> and are highly active, we inferred that relatively low reaction temperature together with the presence of trioctylphosphine (TOP, *vide infra*) could allow a transient existence of such reactive facets, resulting in truncated NCO seeds with 6  $\{100\}$ , 8  $\{111\}$  and 12  $\{110\}$  facets in the infant stage after the nucleation. To achieve a complete formation of PbS NSs, DCE should be introduced into the system immediately as a co-solvent after the addition of S-TOP within no more than 1 min in-between. Although the low boiling-point DCE may be eventually evaporated from the system, it is likely that DCE altered the kinetics of nucleation and crystal growth during the initial stage, promoting adjacent seeds to assemble by merging their  $\{110\}$  surfaces. A postponed addition of DCE (after the reaction mixture turns dark) would result in a mixture of NWs and NSs or even NWs alone. In Figure 3, the PbS NSs prepared in this work are ultrathin ( $< 5\text{-}7$  nm), indicating that their building blocks must be very small prior to the 2D  $\{110\}$ -attachment. Although it was difficult to observe the lattice fringes and diffraction pattern on HRTEM, the Moiré patterns (Figure 3c) formed from a stack of the NSs suggest their high crystalline character. This observation is in agreement with Schliehe's work, that is, the  $\{110\}$ -attachment can only occur among tiny seeds of  $\sim 10$  nm.<sup>24</sup>

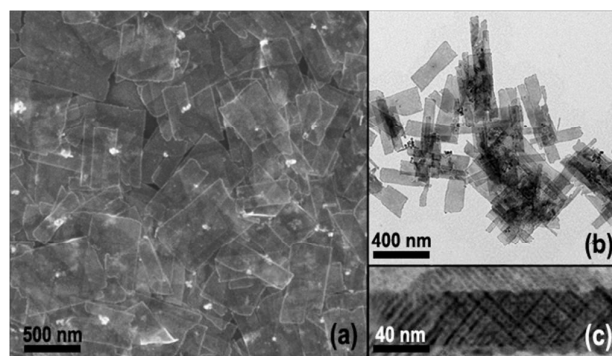


**Figure 3.** EM image of PbS NSs prepared at  $150^\circ\text{C}$  for 7.5 min. (a) SEM image, (b) TEM image, (c) HRTEM image of stacked NSs, showing a Moiré pattern.

The nucleation and growth of NCs can be driven in seconds by the supersaturation of precursor monomers and seeds, respectively, which undergo competing mechanisms before reaching the final product.<sup>3, 20</sup> Upon injection of the lead precursor into a hot organic solvent containing sulphur precursors,  $\text{Pb}^{2+}$  in Pb-oleate will react with  $\text{S}^{2-}$  from S-TOP to

form PbS monomers, while TOP and OAm act as stabilizers for the PbS monomers/seeds. It was reported that TOP plays a determinant role in stabilizing promoted {111} or {110} facets for 1D or 2D nanostructure formation, in the presence of OAm to prevent from aggregation.<sup>31</sup> In contrast, replacement of TOP with an equal amount of OAm in the sulphur precursor resulted in a formation of discrete and large PbS NCBs (~10 nm) with a slight truncation (Figure S3 in SI), producing a distinct difference in the synthetic design of facet-controlled PbS nanoarchitectures. The truncated NCBs are in the process towards developing into perfect NCBs, which is just a matter of tuning the growth time or temperature. The growth completion to “perfect” PbS NCBs in Figure 4a occurred as the reaction temperature increased to 200°C.

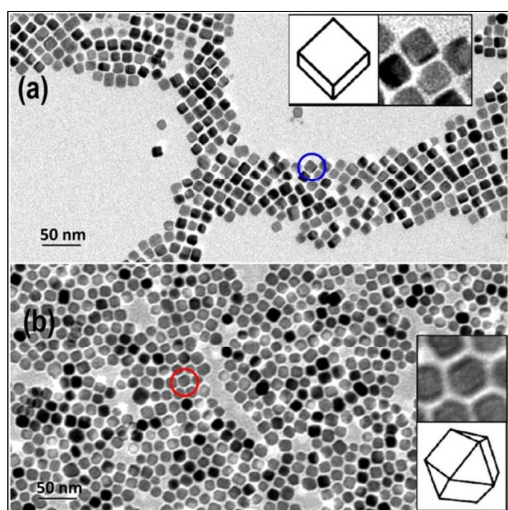
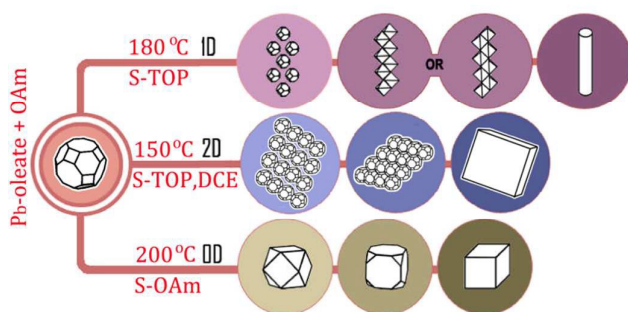


**Figure 4.** TEM images of PbS NCBs grown at 200°C for 7.5 min. (a) without using DCE, the blue circle highlights a typical NCB from <100> direction of view (see the insets); (b) in the presence of DCE, the red circle highlights a six-{100}-sided NC corresponding to a NCO from <100> direction (see the insets).



**Scheme 1.** Schematic illustration of the formation pathways of PbS nanostructures in various dimensionalities.

To further confirm the role of DCE, the recipe for PbS NCB synthesis was modified by introducing DCE as a co-solvent immediately after the S-OAm injection. If DCE could alter the reaction kinetics as discussed in the case of 2D NS synthesis,

the intermediates in-between the nanooctahedra and NCBs should be produced. While other experimental conditions were kept the same, as depicted in Figure 4b, TEM images of six-{100}-sided NC intermediates generated from the DCE-containing system can be apparently identified as those of NCOs. As shown in the selected NCO in the inset of Figure 4b, some PbS NCOs with slanted {100} and {111} facets and their formed edge facing upwards can be apparently identified as reported previously in PbTe system.<sup>32</sup> Due to the absence of TOP, there is no truncated NCO and these perfect NCOs cannot attach together towards a further assembly.

Scheme 1 summarizes all three classes of the growth routes based on our observations. In the first route, PbS nanooctahedra can attach either by their {111} facets to form 1D NWs in the presence of TOP. The NWs can have a zig-zag structure that gradually forms a smooth NW surface. Unless the growth rate along <111> is significantly hindered, the particles will only attach one-dimensionally because the intermediates rapidly disappear before they can further expand to any 2D structure. In the second route, the formation of 2D NSs requires a presence of unstable {110} facets. This could be achieved by lowering the reaction temperature in the presence of TOP and DCE to alter the reaction kinetics in the early growth stage, so that the {110} facets as feedstock are relatively stable for subsequent attachment into a sheet-like structure. When S-TOP is replaced by S-OAm as the sulphur precursors, the formation of {100} facets suppresses that of both {111} and {110} facets and the resultant discrete PbS large NCBs with a slight truncation would not be able to further attach each other due to the lack of TOP,<sup>31</sup> leading to a formation of separate OD NPs.

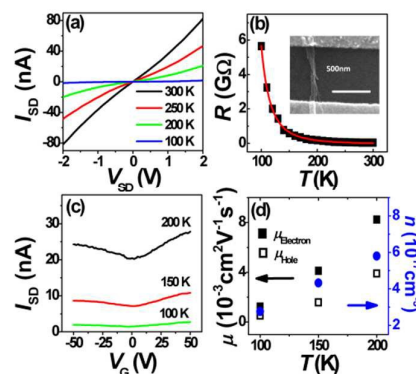


**Figure 5.** (a) The source-drain current-voltage ( $I_{SD}$ - $V_{SD}$ ) behaviour of PbS NWs at various temperatures; (b) Resistance as a function of temperature for the PbS device with its SEM image shown in the inset; (c) The gating voltage dependence of the  $I_{SD}$  measured at a  $V_{SD}$  of 2 V; (d) The mobility and the carrier concentration of the PbS NWs.

As an example of the property exploration on these dimensionality-controlled PbS nanostructures, Figure 5a shows a current-voltage ( $I_{SD}$ - $V_{SD}$ ) behaviour of PbS NWs measured at 300, 250, 200, and 100 K. The linear dependence in the voltage range from -2 to +2 V indicates ohmic contact on PbS NWs and diffusive transport in them. The estimated zero-voltage resistance is shown in Figure 5b with device SEM image shown in the inset. The resistance of the PbS NW device

is  $\sim 30 \text{ M}\Omega$  at 300 K while it increases rapidly up to  $\sim 5.6 \text{ G}\Omega$  at a low temperature of 100 K. Such a rapid increase of the resistance implies strong scattering of carriers transporting in the PbS NWs. The transport ( $R$ - $T$ ) behaviour can be fitted by the thermally activated transport theory of the form  $R = R_0 \exp(E_a/k_B T)$ , where  $R_0$  and the activation energy  $E_a$  are two parameters, and  $k_B$  is the Boltzmann constant. The activation energy of the PbS NWs is evaluated to be about 70 meV. The most interesting result of the PbS NWs is the bipolar gating behaviour that is presented in Figure 5c. For a highly  $p$ - or  $n$ -type doped PbS NWs, the gating effect is more obvious thus the on/off ratio could be up to several orders of magnitudes. In our results, the PbS NWs are close to intrinsic doping thus exhibiting the bipolar gating behaviour. The mobility, extracted from Figure 5c, and the carrier concentration of PbS NWs are shown in Figure 5d. As expected, the carriers suffering strong scattering in PbS NWs reveal very low electron and hole mobility. The carrier concentration for electrons and holes is about  $6 \times 10^{17} \text{ cm}^{-3}$  at 200 K. It is clear that the mobility and the carrier concentration decrease with a decrease of temperature. Once again, the decreasing trend of the mobility and the carrier concentration confirms the thermally activated and the diffusive transport in the PbS NWs.

## Conclusions

In conclusion, using a wet-chemical synthetic protocol we have demonstrated shape-controlled synthesis of PbS nanoarchitectures in three different classes of morphologies and discussed their possible formation mechanisms. High temperature favours a formation of 1D NWs through a  $\{111\}$ -facet attachment, whereas low temperature with chloride compound DCE promotes a product of 2D NSs via a  $\{110\}$ -facet merging. At an infant stage, TOP is essential for facilitating both  $\{111\}$  and  $\{110\}$ , the high surface energy facets. Without TOP, discrete PbS NCs with a slight truncation would be harvested as predicted. The results suggest that the presence of crystal facets in the small intermediate polycrystalline (seeds) could determinately direct the facilitation of nanoarchitectures with certain morphology and dimensionality, and it is significant to understand their growth mechanisms. There are many unique physical characteristics associated with these PbS nanoarchitectures that are worthy of in-depth investigation and tuning. For instance, the PbS NWs are close to intrinsic doping and exhibit the bipolar gating behaviour. This development of facet-controlled nanocrystal preparation as state-of-the-art building blocks is also essential in processing/manipulation in novel nano-patterns of smart materials such as photovoltaic and sustainability energy-related devices.

## Acknowledgements

This work was partially supported by NSF (DMR-0731382), Analytical and Diagnostics Laboratory (ADL) and General

Motors LLC. W. Loc acknowledges Harpur College "undergraduate research project" support at Binghamton University. We thank Dr. P. Stanley May and Dr. Mary T. Berry at University of South Dakota for their help in using the TEM facility that was obtained through an NSF grant (CHE-0840507).

## Notes and references

1. Y. Sun and Y. Xia, *Science*, 2002, **298**, 2176-2179
2. Y. Xia, Y. Xiong, B. Lim and S. E. Skrabalak, *Angew. Chem. Int. Ed.*, 2009, **48**, 60-103.
3. Y. Yin and A. P. Alivisatos, *Nature*, 2005, **437**, 664-670.
4. Z. Quan, L. Valentin-Bromberg, W. S. Loc and J. Fang, *Chem. Asian. J.*, 2011, **6**, 1126-1136.
5. F. W. Wise, *Acc. Chem. Res.*, 2000, **33**, 773-780.
6. H. W. Hillhouse and M. C. Beard, *Curr. Opin. Colloid Interface Sci.*, 2009, **14**, 245-259.
7. W. Liang, O. Rabin, A. I. Hochbaum, M. Fardy, M. Zhang and P. Yang, *Nano Res.*, 2009, **2**, 394-399.
8. R. D. Schaller and V. I. Klimov, *Phys. Rev. Lett.*, 2004, **92**, 186601.
9. J. Androulakis, C.-H. Lin, H.-J. Kong, C. Uher, C.-I. Wu, T. Hogan, B. A. Cook, T. Caillat, K. M. Paraskevopoulos and M. G. Kanatzidis, *J. Am. Chem. Soc.*, 2007, **129**, 9780-9788.
10. W. Ma, J. M. Luther, H. Zheng, Y. Wu and A. P. Alivisatos, *Nano Lett.*, 2009, **9**, 1699-1703.
11. J. M. Luther, M. Law, M. C. Beard, Q. Song, M. O. Reese, R. J. Ellingson and A. J. Nozik, *Nano Lett.*, 2008, **8**, 3488-3492.
12. W.-k. Koh, S. R. Saudari, A. T. Fafarman, C. R. Kagan and C. B. Murray, *Nano Lett.*, 2011, **11**, 4764-4767.
13. C. B. Murray, D. J. Norris and M. G. Bawendi, *J. Am. Chem. Soc.*, 1993, **115**, 8706-8715.
14. K.-S. Cho, D. V. Talapin, W. Gaschler and C. B. Murray, *J. Am. Chem. Soc.*, 2005, **127**, 7140-7147.
15. A. J. Houtepen, R. Koole, D. Vanmaekelbergh, J. Meeldijk and S. G. Hickey, *J. Am. Chem. Soc.*, 2006, **128**, 6792-6793.
16. W. Lu, J. Fang, K. L. Stokes and J. Lin, *J. Am. Chem. Soc.*, 2004, **126**, 11798-11799.
17. W. Lu, P. Gao, W. B. Jian, Z. L. Wang and J. Fang, *J. Am. Chem. Soc.*, 2004, **126**, 14816-14821.
18. Z. Quan, Z. Luo, W. S. Loc, J. Zhang, Y. Wang, N. Porter, J. Lin, H. Wang and J. Fang, *J. Am. Chem. Soc.*, 2011, **133**, 17590-17593.
19. Z. Quan, W. S. Loc, C. Lin, Z. Luo, K. Yang, Y. Wang, H. Wang, Z. Wang and J. Fang, *Nano Lett.*, 2012, **12**, 4409-4413.
20. J. S. Steckel, B. K. H. Yen, D. C. Oertel and M. G. Bawendi, *J. Am. Chem. Soc.*, 2006, **128**, 13032-13033.
21. Z. Quan, C. Li, X. Zhang, J. Yang, P. Yang, C. Zhang and J. Lin, *Cryst. Growth Des.*, 2008, **8**, 2384-2392.
22. G. B. Bhandari, K. Subedi, Y. He, Z. Jiang, M. Leopold, N. Reilly, H. P. Lu, A. T. Zayak and L. Sun, *Chem. Mater.*, 2014, **26**, 5433-5436.
23. Quality of the three-neck round-bottom flask should be pre-checked carefully, and extreme caution should be taken in this cooling step.
24. C. Schliehe, B. H. Juarez, M. Pelletier, S. Jander, D. Greshnykh, M. Nagel, A. Meyer, S. Foerster, A. Kornowski, C. Klinke and H. Weller, *Science*, 2010, **329**, 550-553
25. S. Acharya, B. Das, U. Thupakula, K. Ariga, D. D. Sarma, J. Israelachvili and Y. Golan, *Nano Lett.*, 2013, **13**, 409-415.
26. F. Xu, X. Ma, L. F. Gerlein and S. G. Cloutier, *Nanotechnology*, 2011, **22**, 265604.
27. N. Wang, X. Cao, L. Guo, S. Yang and Z. Wu, *ACS Nano*, 2008, **2**, 184-190.
28. Z. L. Wang, *Phys. Chem. B*, 2000, **104**, 1153-1175.

29. W. Lu, Q. Liu, Z. Sun, J. He, C. Ezeolu and J. Fang, *J. Am. Chem. Soc.*, 2008, **130**, 6983-6991.
30. S. Y. Jang, Y. M. Song, H. S. Kim, Y. J. Cho, Y. S. Seo, G. B. Jung, C.-W. Lee, J. Park, M. Jung, J. Kim, B. Kim, J.-G. Kim and Y.-J. Kim, *ACS Nano*, 2010, **4**, 2391-2401.
31. J. Joo, H. B. Na, T. Yu, J. H. Yu, Y. W. Kim, F. Wu, J. Z. Zhang and T. Hyeon, *J. Am. Chem. Soc.*, 2003, **125**, 11100-11105.
32. T. Mokari, M. Zhang and P. Yang, *J. Am. Chem. Soc.*, 2007, **127**, 9864-9865.

TOC:



## Dimension-controlled PbS nanoarchitectures prepared in solution